Available online at www.sciencedirect.com

ScienceDirect

Energy Procedia 35 (2013) 102 – 112

Energy Procedia

DeepWind, 24-25 January 2013, Trondheim, NORWAY

Wave–induced characteristics of atmospheric turbulence flux measurements

Mostafa Bakhoday Paskyabi[a,*], Martin Flügge[a], James B. Edson[b], Joachim Reuder[a]

[a]*Geophysical Institute, University of Bergen, Allégaten 70, N-5007 Bergen, Norway*
[b]*University of Connecticut, Avery Point,1084 Shennocossett Road, Groton, CT 06340, USA*

Abstract

In this paper, we present the air–sea flux of momentum obtained with the eddy correlation method applied to data measured from a moored discus buoy deployed approximately 600 m off a research Air Sea Interaction Tower at Martha's Vineyard Coastal Observatory, Massachusetts during spring 2010. We discuss corrections to account for the wave–induced motion of buoy. Our analysis confirm that the neutral drag coefficient depends upon wave age and wind speed. The data scatter between wind and momentum stress in the low wind speed are significantly larger for those with higher wind speeds. Furthermore, the momentum transfer is investigated using a wave model with sea state dependent drag coefficient. This wave age dependent drag reveals fairly good agreement compared to the observed drag coefficient.

Keywords: air–sea flux, momentum flux, eddy correlation, motion correction, drag coefficient

1. Introduction

The capability of estimating the exchange of mass, momentum, and energy between atmosphere and the ocean depends highly on the quality of measurements made to extract these fluxes across this wavy boundary. The hydrodynamic properties of this complex interface is characterized by introducing a drag coefficient, C_D, or an aerodynamic sea surface roughness, z_0. Due to crucial importance of the wind stress to generate the surface gravity waves and wind–induced ocean circulation, decades of extensive studies have been done to determine C_D and z_0 over the ocean as a function of wave forcing and wind stress.

Jones and Toba (2001) [1] pointed out that the present parameterizations of the drag coefficient over the ocean is far from satisfactory due to the significant uncertainty regarding to the surface gravity wave effects. Drennan et al. 1999 [2] showed that the momentum fluxes are influenced in the vicinity of the sea surface by the presence of swell. Furthermore, they presented that in the pure wind sea, the Monino–Obokhov similarity would appear to hold. Based on laboratory data, Donelan (1987) [3] showed that the long, gentle swell propagating in the wind direction has a substantial effect on the wind sea spectrum. In this study, we

*Corresponding author
Email address: Mostafa.Bakhoday@gfi.uib.no (Mostafa Bakhoday Paskyabi)

doi:10.1016/j.egypro.2013.07.163

investigate preliminarily the mean wind profile and the drag coefficient measurements over the sea surface in the presence of surface gravity waves measured from a moored moving buoy. Although the swell has a significant effect on the overall roughness and drag coefficient, we will not specifically deal with swell effects on the measurements of turbulent fluxes in the present study, and we only report some preliminary results on the wave–turbulence and wave–wind interactions over the sea wavy surface.

In Section 4, we present new data from a moving moored discus buoy under different meteorological conditions and wave forcing. We discuss in the, the corrections for the platform movements and compare eddy correlation fluxes measured from a moving platform before and after corrections with those measured from fixed tower in the vicinity of buoy location. Furthermore, a sea–state drag coefficient is presented in this section based on a wave model. Results are given in Section 5. Finally, we summarize and conclude this study in Section 6.

2. Background

The tangential stress exerted to the ocean surface by wind at some levels above viscous sublayer is expressed by

$$\tau = -\rho_a(\overline{u'w'}\,\hat{\mathrm{i}} + \overline{v'w'}\,\hat{\mathrm{j}}), \tag{1}$$

where ρ_a denotes the air density, $\hat{\mathrm{i}}$, and $\hat{\mathrm{j}}$ represents orthogonal unit vectors. The fluctuating velocity components u', v', and w' are decomposed from instantaneous velocities $u, v,$ and w using Reynolds decomposition method (e.g., $u = \bar{u} + u'$). In this study, we align the x–axis with the wind direction. Thus, we will hold the longitudinal stress component $\tau_x = -\rho_a\overline{u'w'}$ as downstream stress, and $\tau_y = -\rho_a\overline{v'w'}$ as the cross wind stress. The overbars represents time average over periods of order 20 minutes (for our data set). Conventionally, Eq. (1) is parameterized by the following bulk formula

$$\tau = \rho_a C_D U(z)^2, \tag{2}$$

where U is the horizontal mean wind speed at height z above the ocean surface ($U \equiv \bar{u}$). By assuming the momentum flux is constant in the sea surface layer, the vertical velocity profile is given based on Moninon–Obukhov similarity theory by

$$U(z) = \frac{u_*}{\kappa}\left[\ln\frac{z}{z_0} - \psi_m\right], \tag{3}$$

where κ is the von kármán constant, z_0 is the aerodynamic roughness length, and ψ_m denotes the integrated non–dimensional wind gradient, ϕ_m, that is an empirical function of the stability parameter:

$$\xi = \frac{z}{L} = \frac{zg\kappa(\overline{\theta'w'} + 0.61\overline{q'w'}\,\overline{\theta})}{u_*^3\overline{\theta}}, \tag{4}$$

where L is the Obukhov length and $\overline{\theta'w'}$ is the buoyancy flux, $\overline{\theta}$ denotes the mean potential temperature in the surface layer, and g denotes acceleration due to gravitational force. The air–side friction velocity, u_* introduced in Eqs. (3) and (4) is defined through the wind stress magnitude as

$$u_* = \frac{|\tau|}{\rho_a} = \sqrt{(\overline{u'w'})^2 + (\overline{v'w'})^2}. \tag{5}$$

Using dimensional analysis, Charnok 1955 [4] proposed that z_0 can be described as

$$z_0 = \alpha\frac{u_*^2}{g}, \tag{6}$$

where $\alpha = 0.012$ is the Charnok constant. It should be noted that several observations have reported a widely scatter in the value of α.

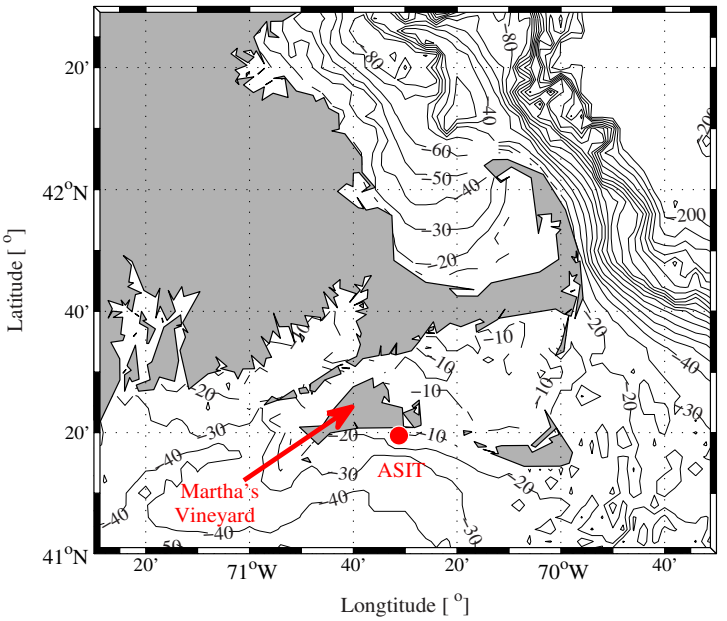

Fig. 1. Bathymetric contours and site map of Martha's Vineyard showing the location of the ASIT frame (bold circle).

A widely used relation for the drag coefficient can be expressed as

$$C_D = [a + bU_{10}] \times 10^{-3}, \tag{7}$$

where $a = 0.8$ and $b = 0.065$ corresponds to a Charnok constant $\alpha = 0.018$. In the data collected during the Risø Air Sea Experiment (RASEX) experiment $a = 0.75$ and $b = 6.7 \times 10^{-2}$ [5], and in the surface wave experiment SWADE, $a = 0.6$ and $b = 7.0 \times 10^{-2}$ for $U_{10} \in (6, 14)$ m s^{-1} [2]. Furthermore, Greenaert et al. 1987 [6] showed that

$$C_D = A\left(\frac{c_p}{u_*}\right)^B, \tag{8}$$

gives a better fit with their data set than relations (6) and (7). In Eq. (8), A and B are coefficients determined by the data, and c_p is the phase speed at peak frequency of wave energy spectrum. Donelan et al. 1993 [7] reported direct observations of wind stress and wave properties during the surface wave experiment SWADE [2]. They obtained the following regression formula for the pure wind sea,

$$z_0 = \sigma A\left(\frac{U_{10}}{c_p}\right)^B, \tag{9}$$

where $A = 6.7 \times 10^{-4}$ and $B = 2.6$ are the regression coefficients. Drennan et al. [8] showed the Charnok parameter α in Eq. (6) depends on the state of the surface waves. Sullivan et al. 2000 [9] and Sullivan et al. 2008 [10] studied effects of swell on the turbulence structure in the overlying airflow by support of direct numerical simulation and large eddy simulation models.

3. Instruments and experimental site

3.1. Data Collection

The observations reported here were made using instruments deployed at the area of the Martha's Vineyard Costal Observatory's (MVCO's) Air Sea Interaction Tower (ASIT) during spring 2010 (Fig. 1). The

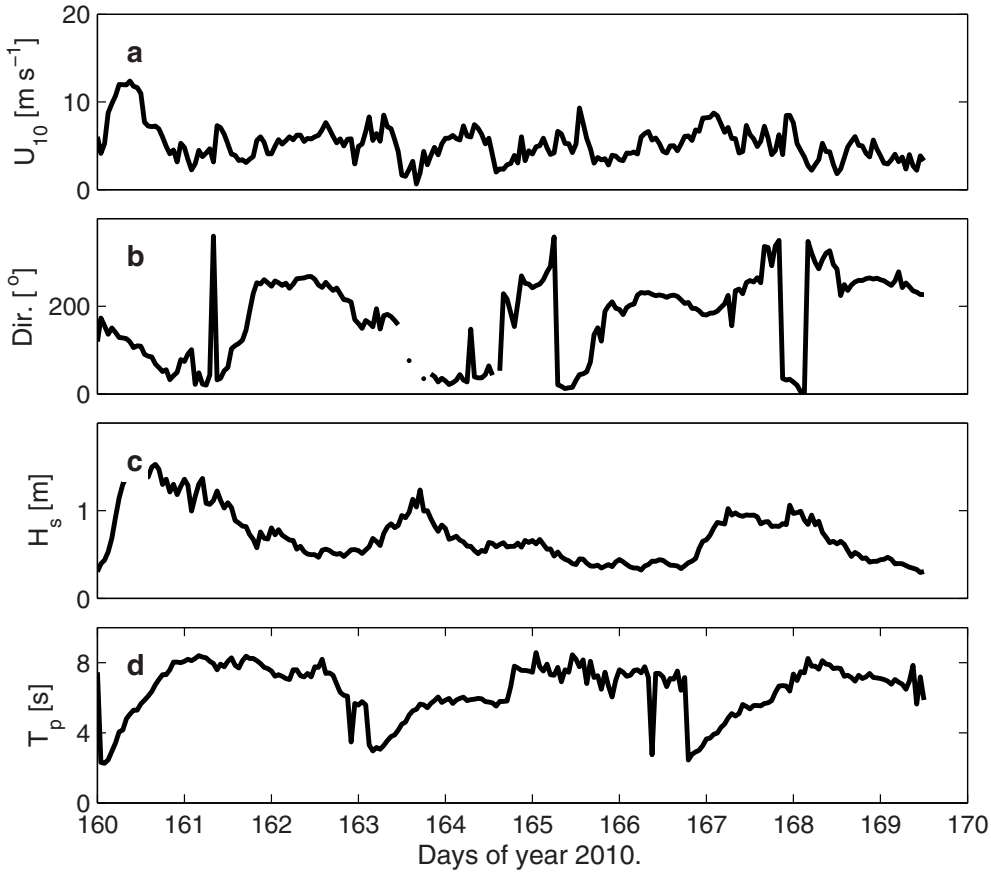

Fig. 2. Environmental conditions at the observation site between days 160 to 170, 2010. a) Wind speed at 10-m height, b) Wind direction, c) significant wave height H_s, and d) peak wave period T_p.

ASIT is located 3.2 km to the south of Martha's Vineyard beach in approximately 16 m of water with the shoreline and bathymetric contours oriented roughly east–west (Fig. 1). A discus buoy has been moored approximately 600 m distance from the ASIT. Both ASIT and buoy were deployed and exposed to the dominant atmospheric forcing and equipped with similar air–sea measurement instruments for the period between days 160–170 during 2010. The wind vector for buoy was measured with a three–axis sonic anenometer at height of 3.76 m above the mean surface. A motion package consisting of three orthogonal pairs of rate gyros and linear accelerometers, and a compass was installed on both the buoy and the tower. This motion data are used to correct measured wind speed vector and temperature data contaminated due to wave–induced platform motion using algorithm given by Edson et al. 1998 [11] and Miller et al. 2008 [12].

3.2. Environmental Conditions

Figure 2 shows wind speed and direction time evolution during the experiment between days 160–170. It reveals one dominant wind regime during period of buoy measurements. Wind blowing from south and southeastern sectors have speeds ranged from 2 to 12 m s^{-1}. Weaker winds blow from northern and northeastern sectors with speed less than 5 m s^{-1} (narrow northern section). Rapid changes in the wind direction occurs on the time scales of about one day that are noticeable features of the local wind variabilities in the

experimental site. Major and minor wind events followed each other during the experiment. Significant wave height and peak wave period are demonstrated in Fig 2-c and d, respectively. Maximum significant wave height, H_s, reaches about 1.5 m and the peak period T_p about 8 s.

4. Wind Stress Calculation Over the Ocean

4.1. Eddy correlation technique

The eddy correlation (EC) technique is based on direct calculation of wind stress as expressed through Eq. (1). There are two major complications for applying this technique: i) contamination induced by platform motion, ii) flow distortion. Since, we are measuring wind in a moving coordinate system, it is crucial to apply correction on the measured wind velocities. Based on the technique proposed by Fujitani 1981 [13] and improved by several researchers such as Edson et al. 1998 [11] and Miller et al. 2008 [12], the corrected wind velocity using motion package sensors is expressed by the following basic equation:

$$\mathbf{V}_{true} = \mathbf{TV}_{obs} + \Omega \times \mathbf{TL} + \mathbf{TV}_{plat}, \tag{10}$$

where $\mathbf{V}_{true}$ is the corrected wind vector in the Earth reference frame, $\mathbf{V}_{obs}$ denotes the measured wind velocity vector relative to the buoy coordinate system, $\mathbf{T}$ is the transform matrix from buoy coordinate to the Earth reference fixed frame of coordinate, $\mathbf{L}$ represents the position vector of the wind sensor with respect to the motion package, and $\mathbf{V}_{plat}$ is the buoy translational velocity vector with respect to the buoy coordinate system. Before applying the EC technique, the corrected velocity vector is rotated into the streamwise wind (i.e. $\bar{v} = \bar{w} = 0$) and then linearly detrended. After these processing stages, the covariance or flux cospectrum are calculated to compute wind stress as

$$\overline{u'w'} = \int_0^\infty Co_{uw}(f)df. \tag{11}$$

Here, the time–spane of each segment to EC estimate is 20 min, Co_{uw} denotes covariance between u and w components of wind speed, and f denotes frequency in Hz.

4.2. Inertial Dissipation Method

In Inertial Dissipation (ID) technique, turbulent fluxes are determined from Turbulent Kinetic Energy (TKE) budget equation which describes the physical processes of generating turbulence [2]:

$$\overbrace{\frac{\partial e}{\partial t}}^{1} + \overbrace{U.\nabla e}^{2} = \overbrace{u_*^2 \frac{\partial U}{\partial z}}^{3} - \overbrace{\frac{g}{T}\overline{w'\theta'}}^{4} + \overbrace{\frac{\partial \overline{w'e}}{\partial z}}^{5} + \overbrace{\frac{1}{\rho_a}\frac{\partial \overline{w'p'}}{\partial z}}^{6} + \overbrace{\varepsilon}^{7}, \tag{12}$$

where $e = 0.5(u'^2 + v'^2 + w'^2)$ is the TKE, term 1 presents the local storage of TKE, the advection of TKE by the mean wind is denoted by term 2. Terms 3, 4, 5 and 6 represent the shear production, buoyancy production/dampening, the vertical turbulent transport, and the pressure correlation term, respectively. The molecular dissipation of TKE is denoted by the last term.

Assuming local storage and advection terms to be negligible, and dividing Eq. (12) by $u_*^3/(\kappa z)$, we obtain:

$$\phi_u - \xi - \frac{\kappa z}{u_*^3}\varepsilon - \phi_t - \phi_p = 0, \tag{13}$$

where

$$\phi_u = \frac{\kappa z}{u_*^3}\frac{\partial \overline{w'e}}{\partial z} \text{ and } \phi_u = \frac{\kappa z}{\rho_a u_*^3}\frac{\partial \overline{w'p'}}{\partial z}.$$

Following Moninon–Obukhov similarity, ϕ_u, ϕ_p, and ϕ_t are expected to be universal functions of ξ. Then from the known dissipation rate of TKE, the wind stress is determined [14].

4.3. Wave and wind stress interaction

Over the sea, the total wind stress can be made up as vector sum of shear stress, τ_s, and wave–induced stress, τ_w. The shear stress is the sum of viscus stress, τ_v, and turbulent stress, τ_t. Then, the total stress can be written as

$$\tau = \tau_v + \tau_t + \tau_w. \tag{14}$$

In general all terms in Eq. (14) depend on height. Under certain conditions in which τ is constant with height, the increase in wave–induced momentum is balanced by a reduction in the turbulent stress. Following Janssen 1991 [16], the wave–dependent total wind velocity is given by

$$U_{10}^{w}(z) = \frac{u_*}{\kappa}\left[\ln\left(\frac{z+z_1}{z_0+z_1}\right) - \psi_m\right]. \tag{15}$$

where z_1 is the wave stress contribution in the effective roughness ($z_e = z_0 + z_1$). The turbulent component is also determined from this effective roughness [17]. The wave stress is expressed as

$$\tau_w = \rho_w \int_0^{2\pi}\int_0^{\infty} \sigma S_{in}(\sigma,\theta) d\sigma d\theta, \quad |\theta_{wind} - \theta| \le \pi/2, \tag{16}$$

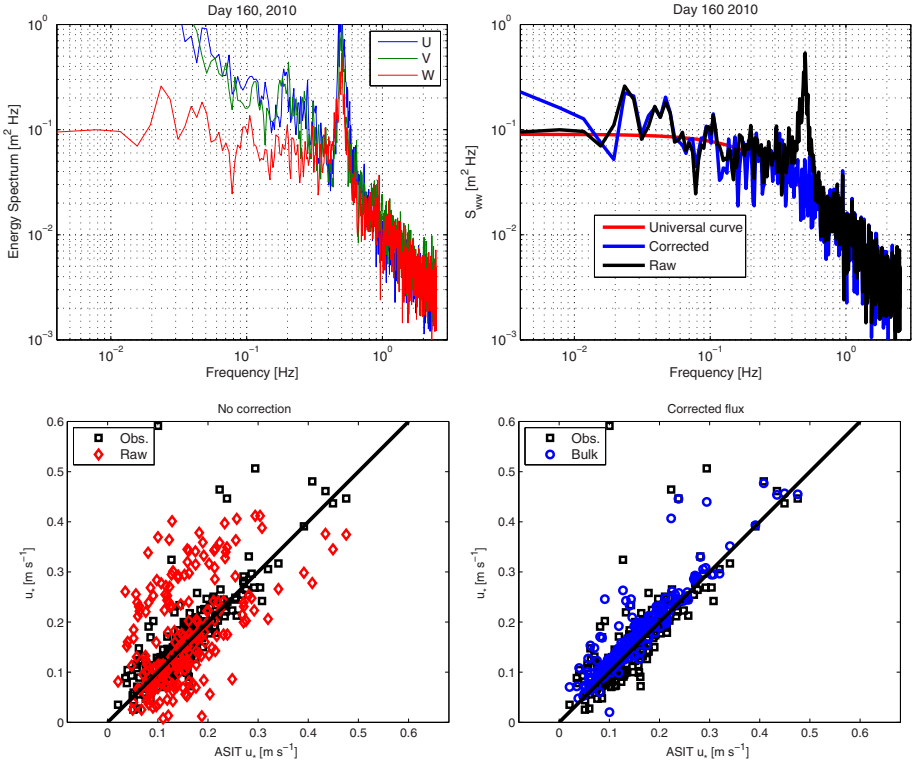

Fig. 3. *Top:left*) Power spectral density of the uncorrected wind components (S_{uu}, S_{vv}, and S_{ww}), *Top:right*) comparisons of power spectral densities between the uncorrected (black line) and the corrected (blue solid) vertical wind components, along with the the empirical formula determined by Kaimal et al. 1972 [15] (red solid), *Bottom:left*) a comparison of the uncorrected bulk friction velocity estimates from the buoy versus those measured by ASIT, and *Bottom:right*) a comparison of the corrected bulk friction velocity estimates from the buoy versus those measured by ASIT.

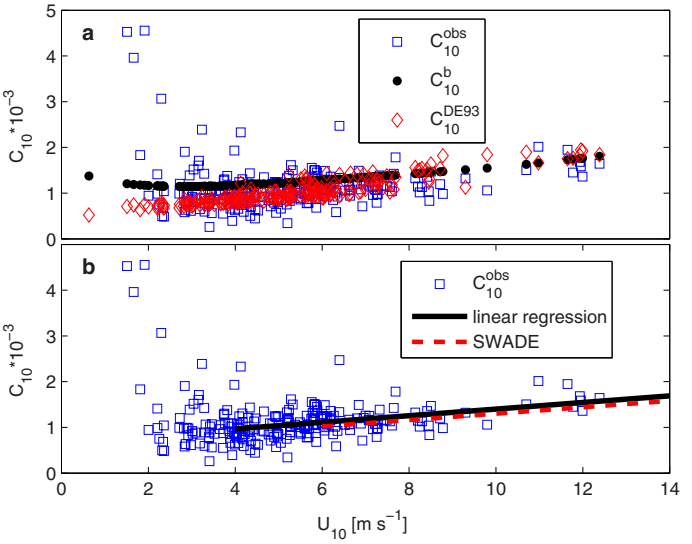

Fig. 4. Neutral drag coefficients (C_{10}) calculated by: a) the EC (squares) method used for buoy data versus U_{10}. Also shown are C_{10} derived from bulk parameterization (dotted line), and estimated from Eq. (9) (diamonds), DE93, and b) the EC method (squares), C_{10} regression curve derived from our data (solid line), C_{10} regression curve derived from SWADE study (dashed line).

where θ_{wind} is the wind direction, θ and σ denote the direction and the angular frequency, respectively. The wind energy input source term is expressed as

$$S_{in}(\sigma,\theta) = \sigma\frac{\rho_a}{\rho_w}\left[\frac{1.2}{\kappa^2}\epsilon\ln^4(\epsilon)\right]\left(\frac{u_*\cos(\theta)}{c_p}\right)E(\sigma,\theta) = \beta_w E(\sigma,\theta),$$

with

$$\epsilon = \left(\frac{u_*\cos(\theta)}{c_p}\right)^2\left(\frac{g\kappa^2 z_e}{u_*^2}\right)\exp\left(\frac{\kappa c_p}{u_*\cos\theta}\right),$$

$$z_e = \frac{z_0}{\sqrt{1-c_0\tau_w/\tau}} \text{ and } z_0 = \frac{\beta_0 u_*}{g\sqrt{1-c_0\tau_w/\tau}},$$

where $\beta_0 = 0.01$ is a constant, and $c_0 = 0.8$ to avoid extensively small decrease of denominator.

5. Results and analysis

In this study, we focus on measurements made using a moored moving buoy deployed in the vicinity of the MVCO's Air–Sea Interaction Tower. The comparisons between fluxes measured by EC and calculated by ID techniques have not been shown here for the sake of brevity and due to the volume limitation. To quantify the effect of motion correction, we implement the motion correction algorithm on buoy data for 10 days between year–days 160 and 170 on 2010. In figure 3-*Top:left*, we compare the turbulent spectra S_{uu}, S_{vv}, and S_{ww} before correction of the data on 11 June 2010. Before platform motion correction, the raw spectra show enhancement of energy at periods 2–5 seconds due to wave–induced platform motion contaminations that should be efficiently removed. In this regard, we apply the motion correction algorithm as suggested in Edson et al. 1998 [11] to remove the wave–induced motions from the buoy wind records. Figure 3-*Top:right* compares between raw vertical velocity spectrum (black solid), and the corrected spectrum (blue solid). This figure shows that the motion–induced spike is effectively removed after the correction procedure. Also shown is the non–dimensional universal curve of vertical wind component [15]. Kaimal et al. 1972 [15]

based on Moninon–Obukhov similarity and observed data derived a set of non–dimensional curves for the power spectra of wind velocity components. Comparison between corrected and universal curve indicates again the skill of correction in removing platform motion contamination from the wind velocity data.

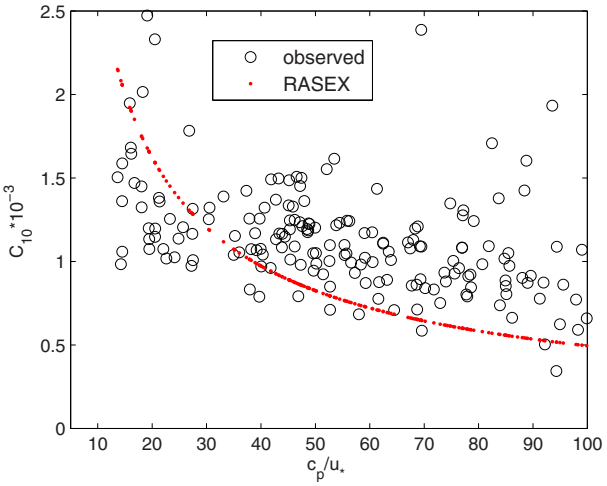

Fig. 5. Nonlinear regression between measured neutral drag coefficient and wave age (open circles), and regression curve based on RASEX study (dotted line).

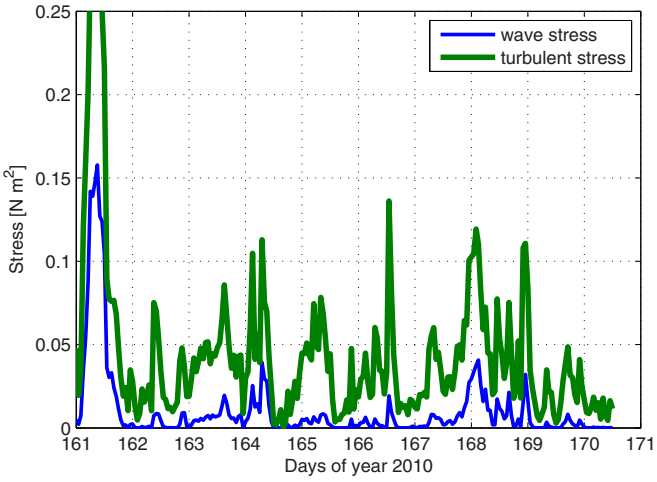

Fig. 6. Time series of the estimated wave, τ_w, and turbulent, τ_t, stresses, respectively.

Calculating the turbulent fluxes using EC technique (Eq. 11) leads to erroneous estimate as expected due to the platform motion associated energy enhancement. Figure 3-*Bottom:left* and *Bottom:right* show comparisons of the friction velocity determined via ASIT with those estimated from the buoy for both uncorrected and motion–corrected wind measurements. The uncorrected results are strongly biased, and mostly represent physically unrealistic behaviors. The corrected friction velocities show a far smaller difference from the measured values by ASIT (Fig. 3-*Bottom:right*).

Figure 4-a shows comparison of observed mean drag coefficient using the EC method (squares) with

those calculated by Eq. (9) (diamonds), DE93, and based on drag coefficient defined by the following z_0 (dotted):

$$z_0 = 0.11\frac{\nu}{u_*} + \alpha\frac{u_*^2}{g}. \tag{17}$$

Here, plots are provided by $\alpha = 0.012$, and ν is the molecular viscosity of air. The indication of upward momentum flux from swell can be seen in the lower wind regions that corresponds with the increase of scatter in the distribution of C_{10}. Note, we use C_{10} to identify drag coefficient at 10 m height afterward in this paper. Furthermore, we discarded the angular characteristic of swell compared to the wind in this study. Observed and estimated drag coefficients decrease monotonically with decreasing wind speed. However, on the average, they generally tend to increase with less scatter as the wind speed increase, because (subsection 4.3), swell is not associated with the local wind field (4-a,b). Figure 4–b includes comparisons of C_{10} measured by the EC method (open circles) with C_{10} regression curve of our data (solid line) and drag coefficient regression curve proposed in SWADE study (dashed line). Linear regression curve of our data correlates highly with SWADE regression curve. The linear regression in Fig. 4–b is obtained with a widely used relation for the drag coefficient $C_D = (a + bU_{10}) \times 10^{-3}$. A best fit is found for $a = 0.9056$ and $b = 0.0590$ with a quite low correlation ($r = 0.4$).

To investigate the dependence between drag coefficient and wave age (c_p/u_*), we compare the observed drag with regression curve of the RASEX experimental data. Figure 5 suggests that the agreement between the observed drag coefficients and the regression curve from RASEX is remarkably good. Although the greatest C_{10} values at the higher wind speeds are under predicted and for greatest wave age the observed drag coefficient reveals overestimation.

Figure 6 shows the time series of τ_w and τ_t during year–days 161-170. Both τ_w and τ_t changes monotically with wind speed especially with a large enhancements during major wind event at early of experiment on day 161.

Comparisons between time series of wind speed at 10 m height are shown in Fig. 7–a computed from Eq. (15), blue solid, Eq. (3), red solid, and measurements from ASIT (black solid). Clearly, there is very good agreement between bulk measurements and corresponding ASIT values. However, there appear

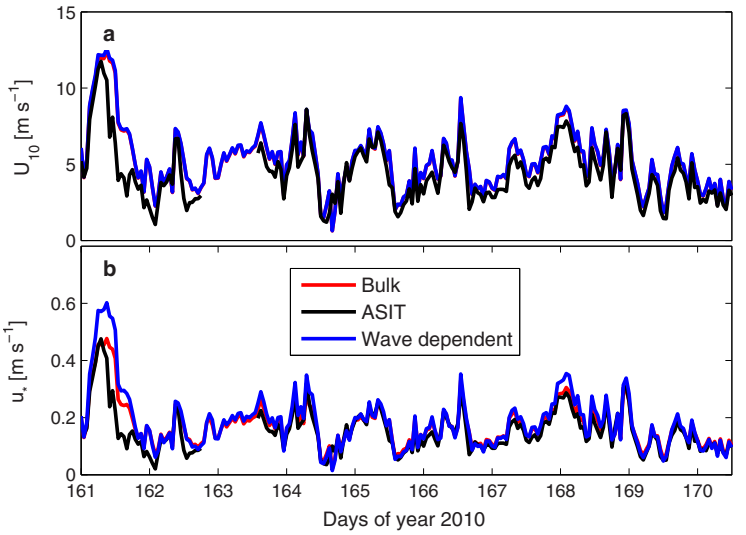

Fig. 7. The top panel shows comparisons between time series of the measured wind velocity at height of 10 m from ASIT (black line) and those estimated using Eqs. (15) and (3) plotted by blue and red lines, respectively. The bottom panel shows the corresponding measured and estimated stresses.

some elevations in the calculations of wind speed and stress derived from wave–dependent relation early of experiment (Fig. 7-a and b).

In Fig. 8, we compare the eddy correlation estimates from ASIT against square friction velocity from the buoy for the same time periods. Friction velocities are computed from wave–dependent formulation and bulk formulation by Eq. (2). Results show direct relation between friction velocities and eddy correlation measurements.

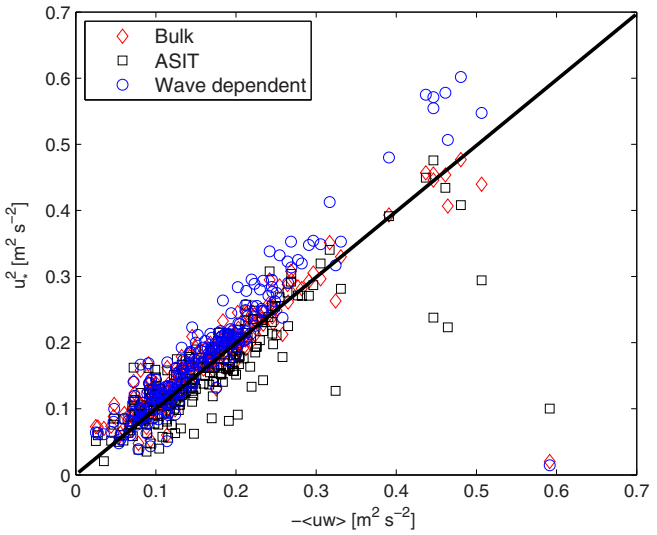

Fig. 8. A comparison of the friction velocity estimates from the moving buoy versus the lateral component of the momentum flux measured from ASIT.

In Fig. 9, the drag coefficient corresponding to Eq. (14) and C_{10} from the bulk aerodynamic method are compared against those measured by ASIT. There is very good agreement between the ASIT measured drag coefficients and bulk estimates.

6. Conclusions

In this study, we used data from a research Air–Sea Interaction Tower at Martha's Vineyard Coastal Observatory, Massachusetts obtained during a field campaign on spring 2010. The tower data provided us an opportunity to examine the skill of motion correction algorithm and properties of the air-sea drag coefficient. We presented here very briefly platform motion correction theory and its application to extract turbulent fluxes and hydrodynamic characteristic of sea surface for our data set. The imposed energy enhancement by platform motion was successfully removed by the correction algorithm. Furthermore, we presented primarily a theory to estimate C_{10} and z_0 using Jannssen 1991 [16] wave stress model. Preliminary results suggests that this technique can be used to estimate hydrodynamic properties of air–sea interface. The discrepancies observed in the results may be explained from excluded important factors in this study such as angular dependency between swell and wind, wave and turbulence separation, need for more accurate platform motion correction techniques, platform vibration effects on turbulent flux measurements, flow distortion, and sonic anenometer angle of attack effects on turbulence measurements.

7. Acknowledgements

The authors would like to thank Scott Miller for his kind help in completing motion correction code. This work has been performed under the Norwegian Center for Offshore Wind Energy (NORCOWE).

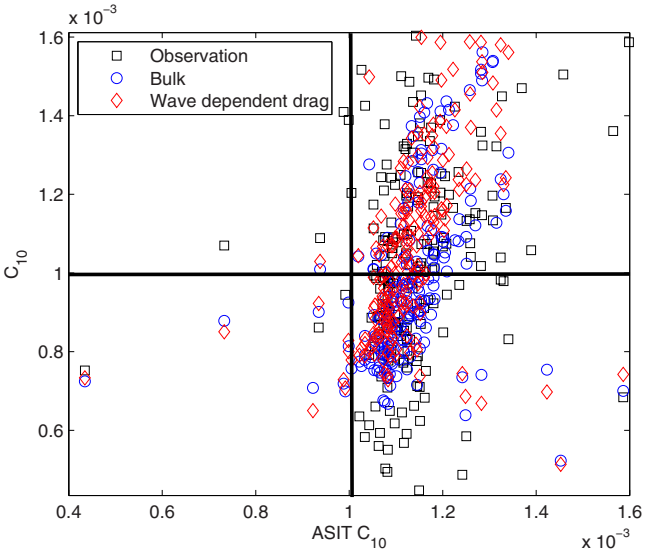

Fig. 9. Comparison of the measured neutral drag coefficient, drag coefficient estimated by Eq. (14), and C_{10} calculated using bulk method from buoy data (vertical axis), with those measured by ASIT (horizontal axis).

References

[1] I. S. F. Jones, Y. Toba, Wind Stress over the Ocean, Cambridge University Press, 2001.
[2] W. M. Drennan, H. C. Graber, M. A. Donelan, Evidence for the effects of swell and unsteady winds on marine wind stress, J. Phys. Oceanogr. 29 (1999) 1853–1864.
[3] M. A. Donelan, The effect of swell on the growth of wind waves, Johns Hopkins APL Tech. Dig. 8 (1987) 18–23.
[4] H. Charnock, Wind stress on a water surface, Quart. J. Roy. Meteor. Soc. 81 (1955) 639–640.
[5] D. Vickers, L. Mahrt, Fetch limited drag coefficients, Bound. Layer Meteor. 85 (1997) 53–79.
[6] G. L. Geernaert, Measurements of the wind stress, heat flux, and turbulence intensity during storm conditions over the north sea, J. Geophys. Res. 92 (1987) 127–139.
[7] M. A. Donelan, F. W. Dobsond, S. D. Smith, On the dependence of sea surface roughness on wave development, J. Phys. Oceanogr. 23 (1993) 2143–2145.
[8] W. M. Drennan, H. C. Graber, D. Hauser, C. Quentin, On the wave age dependence of wind stress over pure wind seas, J. Geophys. Res. 108.
[9] P. P. Sullivan, J. McWilliam, C. H. Moeng, Simulation of turbulent flow over idealized water waves, J. Fluid Mech. 404 (2000) 47–85.
[10] P. Sullivan, J. Edson, T. Hristov, J. C. McWilliam, Large–eddy simulations and observations of atmospheric marine boundary layers above nonequilibrium surface waves, J. Atm. Sci. 65 (2008) 1225–1245.
[11] J. B. Edson, A. A. Hinton, K. E. Prada, J. E. Hare, C. W. Fairall, Direct covariance flux estimates from mobile platforms at sea, J. Atmos. Oceanic Technol. 15 (1998) 547–562.
[12] S. D. Miller, T. S. Hristov, J. B. Edson, C. A. Friehe, Platform motion effects on measurements of turbulence and airsea exchange over the open ocean, J. Atmos. Oceanic Technol. 25 (2008) 1683–1694.
[13] T. Fujitani, Direct measurement of turbulent fluxes over the sea during AMTEX. Pap., J. Meteor. Geophys. 32 (1981) 119–134.
[14] C. W. Fairall, S. E. Larsen, Inertial–Dissipation methods and turbulent fluxes at the air–ocean interface, Boundary Layer Meteor. 34 (1986) 287–301.
[15] J. C. Kaimal, J. C. Wyngaard, Y. Izumi, O. R. Cote, Spectral characteristics of surface layer turbulence, Quart. J. Roy. Meteor. Soc. 98 (1972) 563–589.
[16] P. A. E. M. Janssen, Quasi–linear theory of wind–wave generation applied to wave forecasting, J. Phys. Oceanogr. 21 (1991) 1631–1642.
[17] M. Bakhoday-Paskyabi, I. Fer, A. D. Jenkins, Surface gravity wave effects on the upper ocean boundary layer: modification of a one-dimensional vertical mixing model, Cont. Shelf Res. 38 (2012) 63–78.